Bi_2O_3@Carbon Nanocomposites for Solar-Driven Photocatalytic Degradation of Chlorophenols

Qiang Hao†, Yiwen Liu†, Tong Chen‡, Qingfeng Guo§, Wei Wei†, and Bing-jie Ni*†

†Centre for Technology in Water and Wastewater, School of Civil and Environmental Engineering, University of Technology Sydney, Sydney, NSW 2007, Australia

‡ School of Materials Science and Technology, China University of Geosciences Beijing. Beijing, 100083, China

§ School of Gemmology, China University of Geosciences Beijing. Beijing, 100083, China

***Corresponding author:**

Tel.: +61 295147401; E-mail: bingjieni@gmail.com

Keywords: Bi_2O_3; nanocomposite; photocatalyst; chlorophenols; SPR effect

Abstract

Chlorophenols are corrosive and toxic in water environment, which have arisen increasing concerns and urge solar-driven technique with highly efficient photocatalysts for green remediation. Coupling photocatalysis with surface plasmon resonance (SPR) effect is a practical solution to boosting the utilization of solar light in the infrared region, meanwhile improving the overall performance of the photocatalysts. However, it is still lack of a facile and green strategy to synthesize metallic non-noble bismuth (Bi^0)-based photocatalysts. Herein, we report smart $Bi/Bi_2O_3/C$ composites with high performance for photocatalytic degradation of 2,4-dichlorophenol. Advanced characterizations such as X-ray Diffraction (XRD), Fourier transform infrared spectroscopy (FTIR), X-ray photoelectron spectroscopy (XPS) and high-resolution transmission electron microscopy (HRTEM) are applied to analyze the morphology and structure of the prepared materials. The photodegradation rate of the hybrid is significantly enhanced compared with the sole counterparts, which is 1.60-fold of Bi_2O_3 and 2.47-fold of g-C_3N_4. The synthesized Bi/C-2 exhibits excellent stability without decline in activity after four cycles. The SPR effect of Bi is identified to account for the strengthen photo-reactivity. Moreover, the relatively high utilization efficiency of solar energy and rapid separating rate of photogenerated electron and hole pairs helped to enhance the photocatalytic performance synergistically.

1. Introduction

Chlorophenols are essential chemical raw materials, which have been comprehensively applied in commercial scales of herbicides, pharmaceutical intermediates, wood preservatives and pesticides.[1-3] Hence, chlorophenols have been discovered to enter and accumulated in the aquatic environment ubiquitously. However, chlorophenols are corrosive and toxic, which are harmful to the skin, eyes and respiratory system of human beings.[4] As a major water pollutant nowadays, chlorophenol contamination has arisen increasing concerns and urge a highly efficient solution for chlorophenols purification.[5-6] Although adsorbents are employed to concentrate and separate chlorophenols in water physically, the micro-contaminants are just transferred to another phase and not wholly eliminated.[7-9]

Photocatalysis in advanced oxidation technologies can utilize the photogenerated charge carriers to produce reactive radicals with strong oxidation capacity.[10-16] Different from adsorption, photo-oxidation can mineralize the organic pollutants into harmless inorganic salts, carbon dioxide and water.[17-21] This technology also bears a host of merits, such as environmental friendliness, low cost, long life and extensive universality, inspiring an increasing number of studies on wastewater treatment by photocatalysts.[22-26] Several typical photocatalysts such as titanium dioxide (TiO_2), bismuth phosphate ($BiPO_4$) and zinc oxide (ZnO) exhibit strong oxidation ability, however, they can only absorb ultraviolet light that accounts for only 4% of natural solar light.[27-29] To improve the utilization efficiency of solar energy, visible-light-response photocatalysts have thrust into the limelight on the stage of environmental sciences in the past few decades.[30-32]

Bismuth oxide (Bi_2O_3) is a bismuth-based semiconductor material. Compared with $BiPO_4$, bismuth silicate (Bi_2SiO_5) or bismuth oxychloride (BiOCl), Bi_2O_3 has a simpler component which can be synthesized without complex procedures.[33-36] More importantly, Bi_2O_3 possess a band gap narrower than 2.8 eV, suggesting that it can be excited by visible light.[37] Bi_2O_3 can present in four phases including α, β, γ and δ phase. α-Bi_2O_3 and δ-Bi_2O_3 are low-temperature-stable phase and high-temperature-stable phase, respectively, and the other two are high-temperature metastable phases.[38-39] Among them, α-Bi_2O_3 is more stable than the other phases, affording it a better application prospect. The valence band of α-Bi_2O_3 is about 3.14 eV (vs. NHE) and the comparatively positive valence implies that α-Bi_2O_3 is suitable to be engaged in photooxidation.[40] However, the photogenerated electrons can rapidly reunite with holes, which severely limits the application of α-Bi_2O_3.

Previously several strategies have been used to modify the texture and/or chemical composition of Bi_2O_3 to optimize the electronic structure and conductivity to overcome the limitation, such as elements doping, constructing heterojunctions and plasma modification.[39-46] Reddy et al. prepared Sm^{3+}-doped Bi_2O_3 via a hydrothermal approach which impressively enhanced the catalytic activity for the narrowed bandgap.[41] Wu et al. synthesized Fe^{3+}-doped Bi_2O_3 films by a sol-gel method and increased photodegradation efficiency was improved because of the increased specific surface area and higher light utilization.[42] Moreover, constructing Bi_2O_3 based heterojunctions such as BiOCl/Bi_2O_3, Bi_2O_3/TiO_2, Bi_2O_3/$BaTiO_3$ can also assist to improve the photocatalytic performance of Bi_2O_3.[43-45] Nevertheless, the synthetic methods of elements doping and heterojunction are sophisticated and the composition and property of the derived materials are complicated. The decoration of surface plasmon resonance

(SPR) responsive noble metals such as platinum (Pt), gold (Au) or silver (Ag) is an effective way to enhance the photocatalytic activity of Bi_2O_3.[46-48] However, noble metals are too expensive to be employed in scaling-up applications. In contrast, Dong et al. found that metallic bismuth was a semimetal element which manifests the similar plasmonic property.[49-51] Compared with noble metals, bismuth is much low-cost, less toxic, and more earth-abundant. More importantly, metallic bismuth has direct plasmonic photocatalytic performance and it can be applied as cocatalyst to accelerate the separating rate of photogenerated electron-hole pairs.[50] Typically, metallic bismuth in the hybrids was synthesized by using sodium borohydride as reducing agent, which is not environmental-friendly.[52-53] In other works, a large amount of ethylene glycol is used as the solvent and reducing agent to obtain metallic Bi, despite its hypertoxic potential.[54-55] Under such circumstance, a facile and green method to synthesize metallic Bi^0-based catalysts with excellent photocatalytic activity for chlorophenols degradation is highly desired and has yet been reported.

Herein, we propose a novel approach for the facile synthesis of $Bi/Bi_2O_3/C$ composite photocatalyst with enhanced catalytic activity for degradation of 2,4-dichlorophenol (2,4-DCP). The morphology and structure of the prepared materials are comprehensively characterized. The potential mechanisms for improved catalytic performance are then analyzed. The stability of the materials is evaluated. The findings of this work are expected to envisage in-depth insights into the synthesis and application of Bi^0 based photocatalyst for organic wastewater purification.

2. Materials and methods

2.1 Synthesis of materials

Bismuth nitrate pentahydrate and dicyandiamide are both analytical reagents and bought from Sinopharm Group without further purification. Bismuth nitrate pentahydrate was dried at 60 °C for 2 h to remove the crystal water. After that, the obtained bismuth nitrate was heated to 540 °C in 2 h and calcined at 540 °C for 4 h. The obtained yellow powder is α-Bi_2O_3. The g-C_3N_4 was successfully synthesized by the facile thermal polymerization of dicyandiamide, and the heating condition and temperature is the same as the preparation of α-Bi_2O_3. The Bi/Bi_2O_3 composite materials are prepared as follow. Firstly, different amount of bismuth nitrate pentahydrate and dicyandiamide are weighted and located in an agate mortar. Then they are ground and mixed uniformly. After that, the mixture was transferred into a 50-mL corundum crucible, calcined at 540 °C for 4 h (Scheme 1). The amount of precursor is 5 g and the mass ratio of bismuth nitrate pentahydrate and dicyandiamide are 4:1, 1:1, 2:3 and 1:4. The obtained powder samples are finely ground and denoted as Bi/C-1, Bi/C-2, Bi/C-3 and Bi/C-4. During the synthesis process, all the heating atmospheres were air.

Scheme 1. Schematic Illustration of the Synthesis of Bi2O3@Carbon Nanocomposites

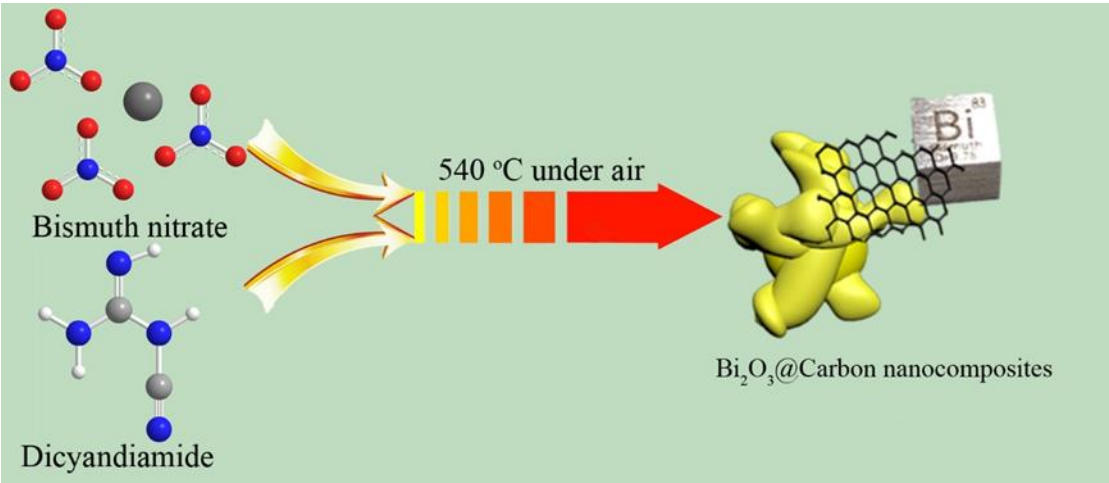

2.2 Characterizations

(Supporting information part 1.)

2.3 Photocatalytic activity tests

(Supporting information part 2.)

2.4 Cycling stability

The cycling stability of Bi/C-2 was tested as follow: after the test of photocatalytic activity, the powder catalyst was collected, which was washed with the mixture of water and ethanol for 3 times each. After that, the powder was dried at 60 °C for 12 h and reused as photocatalyst as mentioned above. During the stability test, the loss of the powder catalyst cannot be avoided. Thus we use 350 mg of samples and seven cuvettes under the same condition at first. After the first cycle, the collected powder can be used to repeat the photodegradation for five cuvettes. After the second cycle, the amount of catalyst can be used in three cuvettes for the parallel test. In the fourth cycle, the rest sample was still enough for one cuvette.

2.5 Trapping experiment

Trapping experiment was used to explore what the active species is during the reaction progress. Isopropanol (IPA) and sodium sulfite (Na_2SO_3) were used as the capture of hydroxyl radical and holes. Nitrogen (N_2) was applied to exclude oxygen and stop forming superoxide radicals. The flow rate of N_2 used during trapping experiment was 20 mL/min. The concentration of IPA and Na_2SO_3 in the 2,4-DCP solution was 0.1 mmol/L. The other details are as same as the test of photodegradation.

3. Results and discussion

3.1 Structure and morphology

XRD patterns are first tested to know the crystal structure of the prepared samples. In Fig. 1, g-C_3N_4 (JCPDS 87-1526) has two distinct diffraction peaks at 13.1 and 27.1°, which are attributed to the (100) and (002) crystal plane diffraction peaks, respectively. The XRD pattern of α-Bi_2O_3 (ICSD 01-071-0465) matches the standard card perfectly. With a different mass ratio of raw materials, the component of obtained samples is different. The main component of Bi/C-1 and Bi/C-2 are α-Bi_2O_3, and they also contain a certain amount of metallic Bi (ICSD 01-077-7112) and remaining organic carbon. As for Bi/C-3 and Bi/C-4, these samples contain β-Bi_2O_3 (ICSD 01-077-5341), metallic Bi, incompletely polymerized dicyandiamide and un-polymerized carbons.

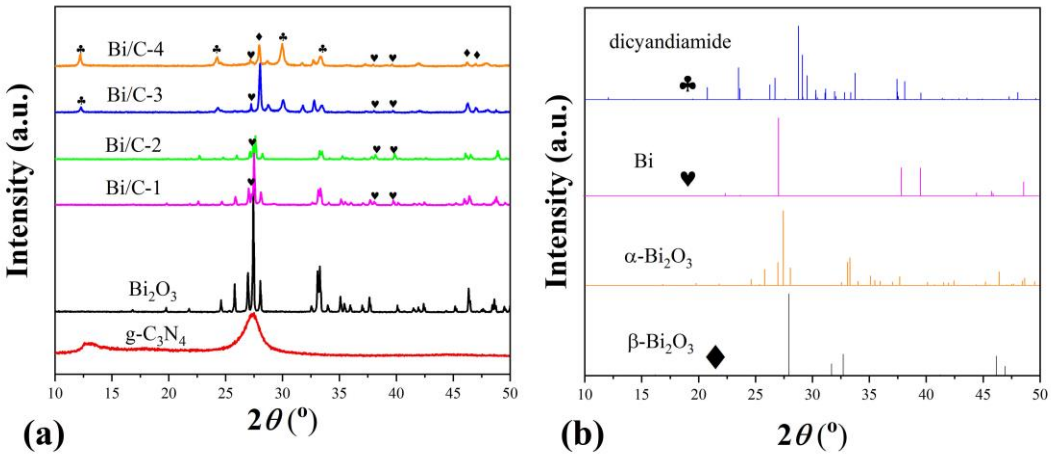

Fig. 1. XRD patterns of g-C_3N_4, Bi_2O_3 and Bi/C composite samples (a), and the XRD standard card of α-Bi_2O_3, β-Bi_2O_3, Bi and dicyandiamide (b).

FTIR of g-C_3N_4, Bi_2O_3 and Bi/C composite samples are then tested to further confirm the component of prepared samples (Fig. 2). For Bi_2O_3, Bi/C-1 and Bi/C-2, the components are mainly inorganic materials and they do not have apparent peaks in the FTIR spectroscopy. The FTIR of g-C_3N_4 fits well with the previous works.[13] While for

Bi/C-3 and Bi/C-4, they have two apparent peaks at 2155 and 1980 cm^{-1}, attributing to the unbroken C≡N of dicyandiamide and newly formed –N=C=O respectively. The peaks are utterly different from g-C_3N_4. Compared with g-C_3N_4, Bi/C-3 and Bi/C-4 have much weaker peaks at 1318 and 1403 cm^{-1} (the aromatic C-N stretching). The strong and sharp peak at 805 cm^{-1} is the bending vibration of s-triazine. According to the FTIR spectroscopy, it can be concluded that the main component of Bi_2O_3, Bi/C-1 and Bi/C-2 are inorganic, while Bi/C-3 and Bi/C-4 are mainly organic. Due to the existence of Bi_2O_3, the polymerization of dicyandiamide is hindered and the C≡N bond is not broken. Although they can form some s-triazine, they are entirely different from g-C_3N_4 and are inactive.

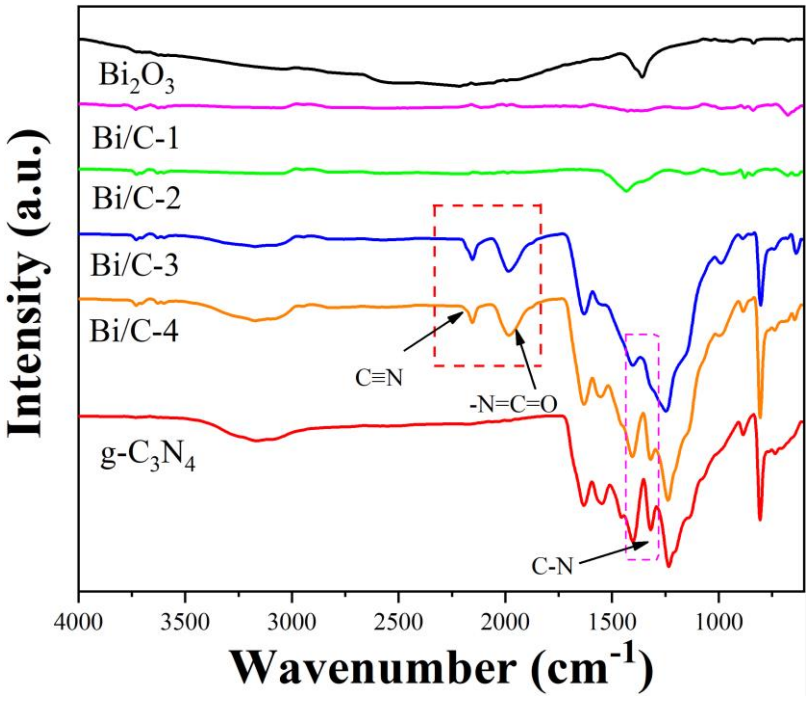

Fig. 2. FTIR of g-C_3N_4, Bi_2O_3 and Bi/C composite samples.

XPS spectra are used to explore the elements and valence states of the derived materials. Fig. 3 shows the XPS high-resolution surveys of C 1*s*, N 1*s*, O 1*s*, and Bi 4*f* for g-C_3N_4, Bi_2O_3 and Bi/C-2. The sp^2 carbon in Fig. 3a is from instrument calibration carbon and

the peak of Bi/C-2 at 288.9 eV is attributed to the C=O groups on the surface.[56] g-C_3N_4 has two peaks at 288.8 and 288.2 eV, both assigning to the sp^2 hybridized C–N bonds. Meanwhile, three peaks at 404.3, 400.6 and 398.8 eV of N 1*s* are accordingly attributed to the π-excitation, the bridging N atoms in $N(C)_3$ and sp^2 N in triazine rings.[57] Nitrogen has not been detected in Bi_2O_3 and Bi/C-2. Fig. 3c is the narrow spectra of O 1*s*. The peaks at 529.0 and 530.4 eV are attributed to the Bi–O bonds. Bi/C-2 have two more peaks at 530.9 and 534.7 eV than Bi_2O_3 due to the remaining organic carbon.[58] From the results of XRD, we confirmed that Bi/C-2 contained some metallic Bi, which is further confirmed by the weak peaks at 161.7 and 156.5 eV.[59]

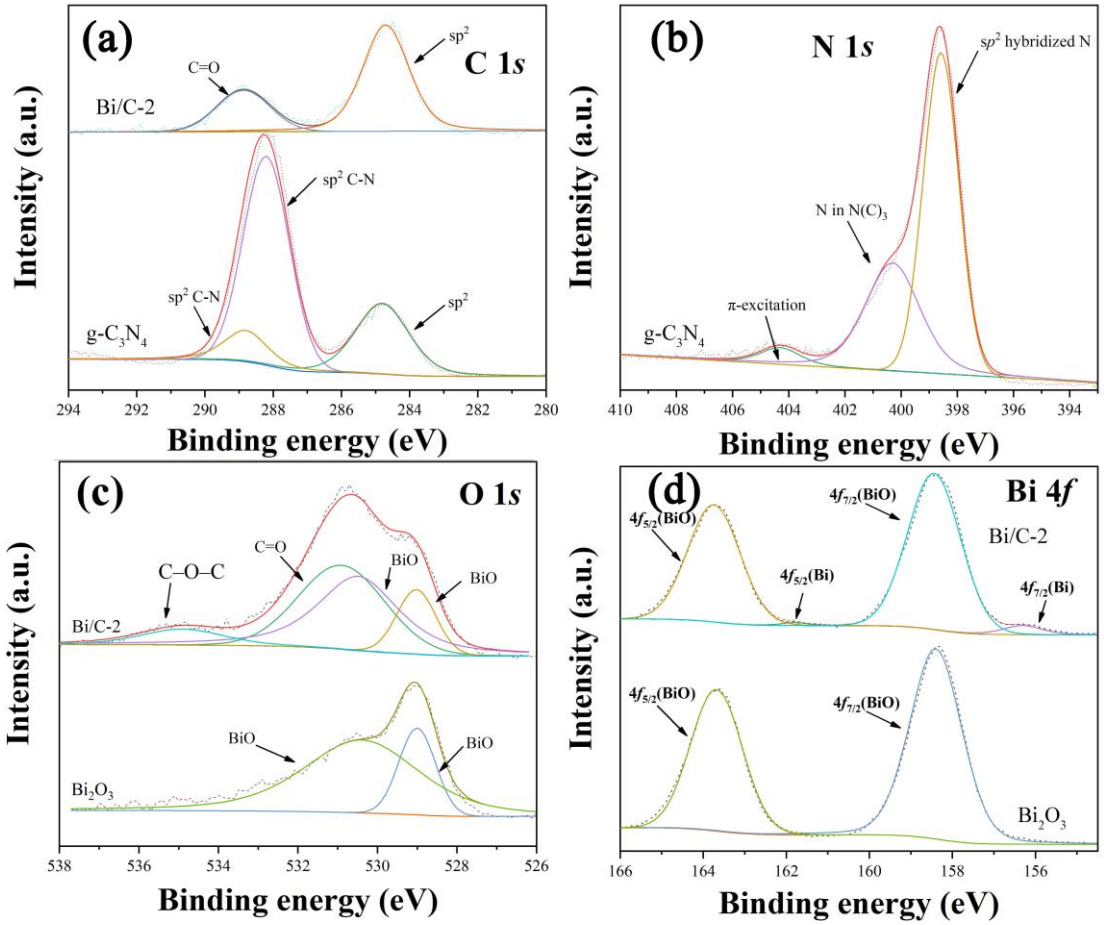

Fig. 3. XPS spectra of g-C_3N_4, Bi_2O_3 and Bi/C-2: the narrow spectra of C 1*s* (a), N 1*s* (b), O 1*s* (c) and Bi 4*f* (d).

Finally, HRTEM is employed to explore the morphology and structure of Bi/C-2. In Fig. 4a the morphology of the sample presents an irregular wormlike shape. Fig. 4b is the detailed crystal lattice on the edge of the particle, in which the lattice spacings of 0.449 and 0.328 nm corresponded to the (110) crystal plane of α-Bi_2O_3 and (012) lattice plane of Bi. On edge, some amorphous part could be clearly observed, which should be the remaining organic carbons.

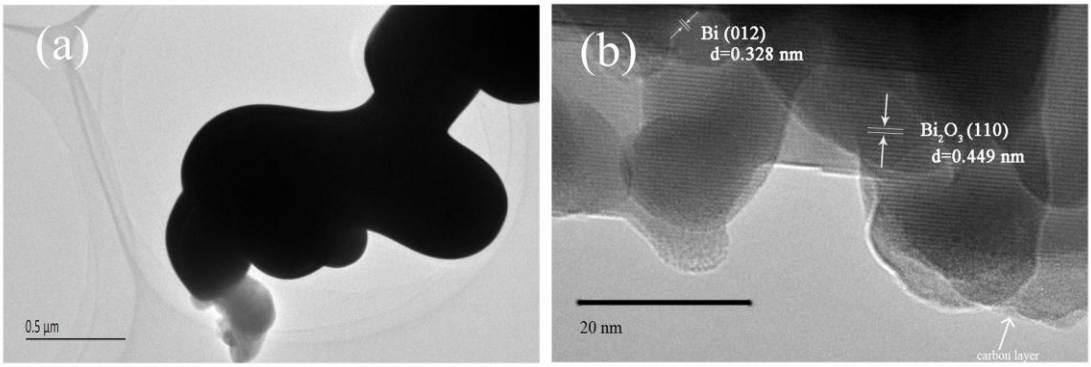

Fig. 4. TEM (a) and HRTEM (b) images of Bi/C-2

According to the above results, the component of Bi/C composite materials can be confirmed. The main component of Bi/C-1 and Bi/C-2 are α-Bi_2O_3, bearing a small proportion of metallic Bi and the carbon layers. As for Bi/C-3 and Bi/C-4, these samples contain β-Bi_2O_3, metallic Bi, and incompletely polymerized dicyandiamide.

3.2 Photocatalytic activity and stability

The photodegradation of 2,4-DCP (simulated sunlight) was used to evaluate the photocatalytic performance of prepared Bi_2O_3, g-C_3N_4 and Bi/C composite samples. As shown in Fig. 5a, the 2,4-DCP concentration gradually decreased during the time course. Bi/C-1 and Bi/C-2 demonstrated better photocatalytic activities than g-C_3N_4 and Bi_2O_3.

The pseudo-first-order rate constant k of Bi/C-2 is 0.22 h^{-1}, which is 1.60 times as Bi_2O_3 and 2.47 times as g-C_3N_4, indicating that the photocatalysis of Bi/C-2 has been significantly enhanced.

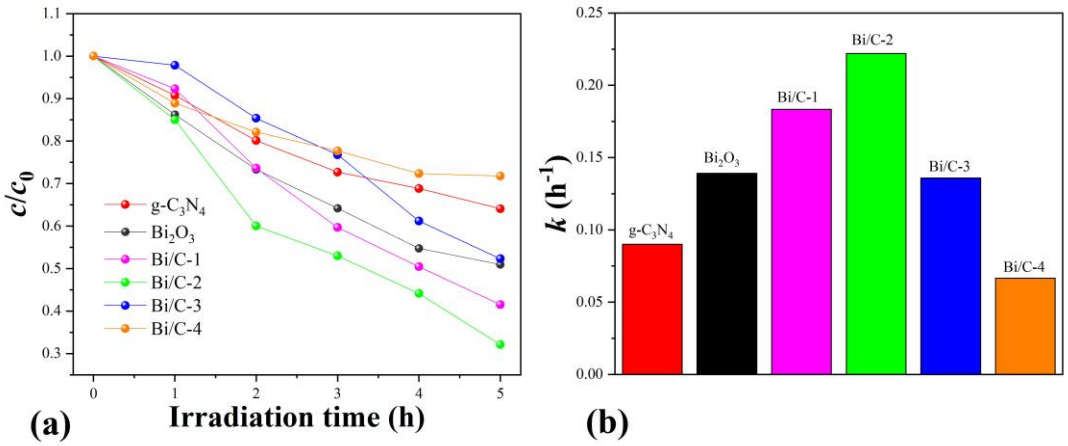

Fig. 5. Photocatalytic activity of g-C_3N_4, Bi_2O_3 and Bi/C composite samples: (a) the change of concentration and (b) pseudo-first-order rate constant k.

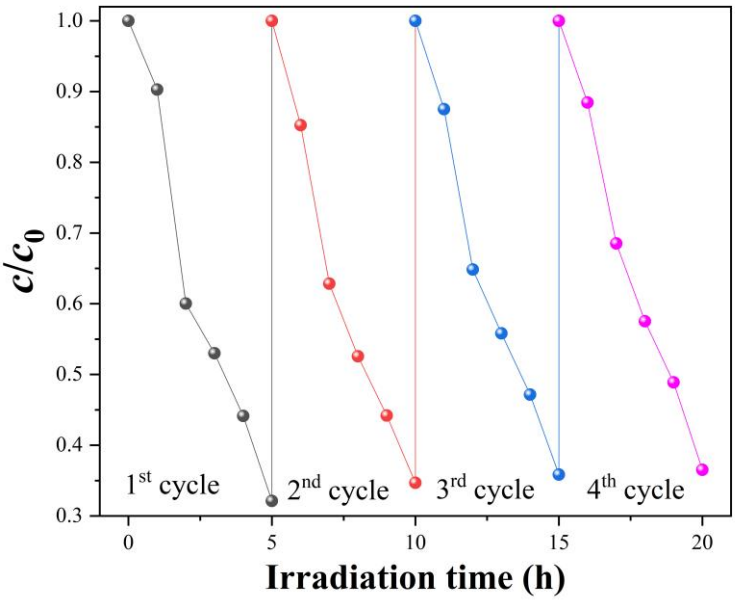

Fig. 6. Cycling stability of Bi/C-2 on the degradation of 2,4-DCP

Cycle stability is also an important property of photocatalysts. Fig. 6 is the cycle

stability of Bi/C-2. In four cycles, the catalytic activity of Bi/C-2 maintains high efficiency without the dramatic decline in degradation rate, indicating that the superior stability of Bi/C-2 in photocatalysis.

3.3 Photocatalytic mechanisms studies

The optimized physiochemical and electronic properties of the novel hybrid structure in Bi^0/Bi_2O_3/Carbon was systematically investigated toward the promoted photocatalysis. UV-vis DRS is used to estimate the light-absorption capacity of the derived photocatalysts. As shown in Fig. 7, the band gap is 2.63 eV for g-C_3N_4 and it is 2.76 eV for Bi_2O_3, indicating that they can both be excited by visible light (In Fig. 7b, $h\nu = E$, E is photon energy and it is proportional to its frequency, ν. The constant of proportionality, h, is known as the Planck constant). However, the visible light utilization is not high. When bismuth nitrate pentahydrate and dicyandiamide are calcined together, the obtained Bi/C composites exhibited much a stronger wave-band absorption in visible light region than g-C_3N_4 and Bi_2O_3, because the black carbon and metallic Bi can significantly improve photon absorption. The enhanced light absorption is beneficial for solar light utilization and photocatalytic activity.

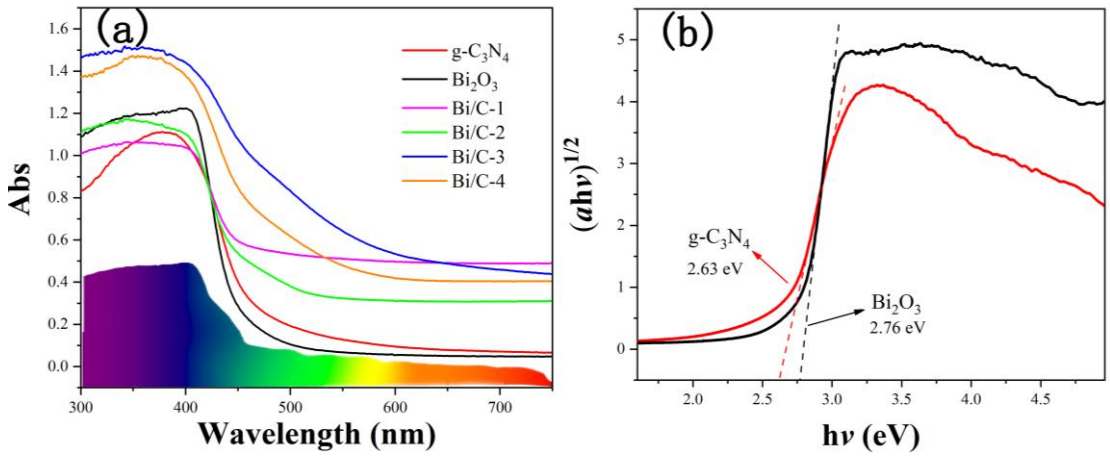

Fig. 7. UV-vis DRS of g-C_3N_4, Bi_2O_3 and Bi/C composite samples (a), and the bandgap of g-C_3N_4 and Bi_2O_3 (b).

Additionally, photocurrent is tested to elucidate the transfer and separating dynamics of photoinduced electrons. The higher photocurrent response implying a higher separation speed of photogenerated electron and hole pairs.[52] Fig. 8a is the photocurrent responses of Bi_2O_3, g-C_3N_4 and Bi/C-2 under simulated sunlight irradiation. All the tested samples have rapid photocurrent when the Xe light is on. The current intensity of Bi/C-2 is much higher than those of g-C_3N_4 and Bi_2O_3, indicating Bi/C-2 has higher separating rate of photoinduced charge carriers. EIS of Bi_2O_3, g-C_3N_4 and Bi/C-2 are shown in Fig. 8b. The arc radius of Bi/C-2 in the EIS plots is much shorter than that of g-C_3N_4 and Bi_2O_3, suggesting that Bi/C-2 manifests a better conductivity contrasted to g-C_3N_4 and Bi_2O_3. This is beneficial for the separation and transport of photoinduced charge carriers (electron and hole) in the photochemical reactions.

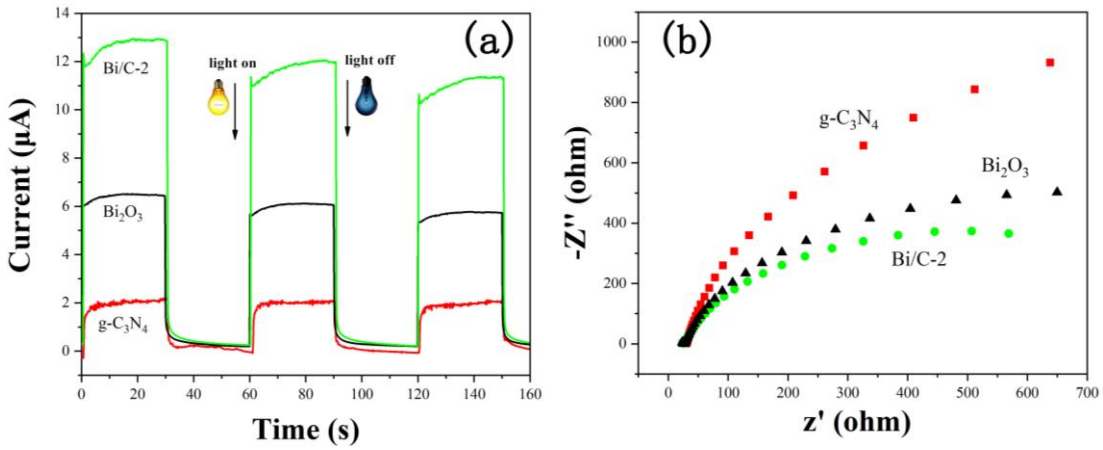

Fig. 8. Photocurrent responses (a) and electrochemical impedance spectroscopy (b) of g-C_3N_4, Bi_2O_3 and Bi/C-2

The PL spectra are also applied to elucidate the recombination rate of photoinduced electron and hole pairs. A stronger PL spectra intensity implies a faster recombination speed of photo-excited electrons and holes. As shown in Fig. 9a, g-C_3N_4 has the

strongest PL spectra intensity, indicating that it has the most rapid reunion speed of charge carriers. The PL spectra intensities of Bi_2O_3 and Bi/C-2 are much lower than that of g-C_3N_4, whereas Bi/C-2 achieved the lowest PL spectra intensity. The results of photocurrent, EIS and PL can confirm that the reunion of photoinduced electrons and holes is restrained by the inducing of Bi and carbon.

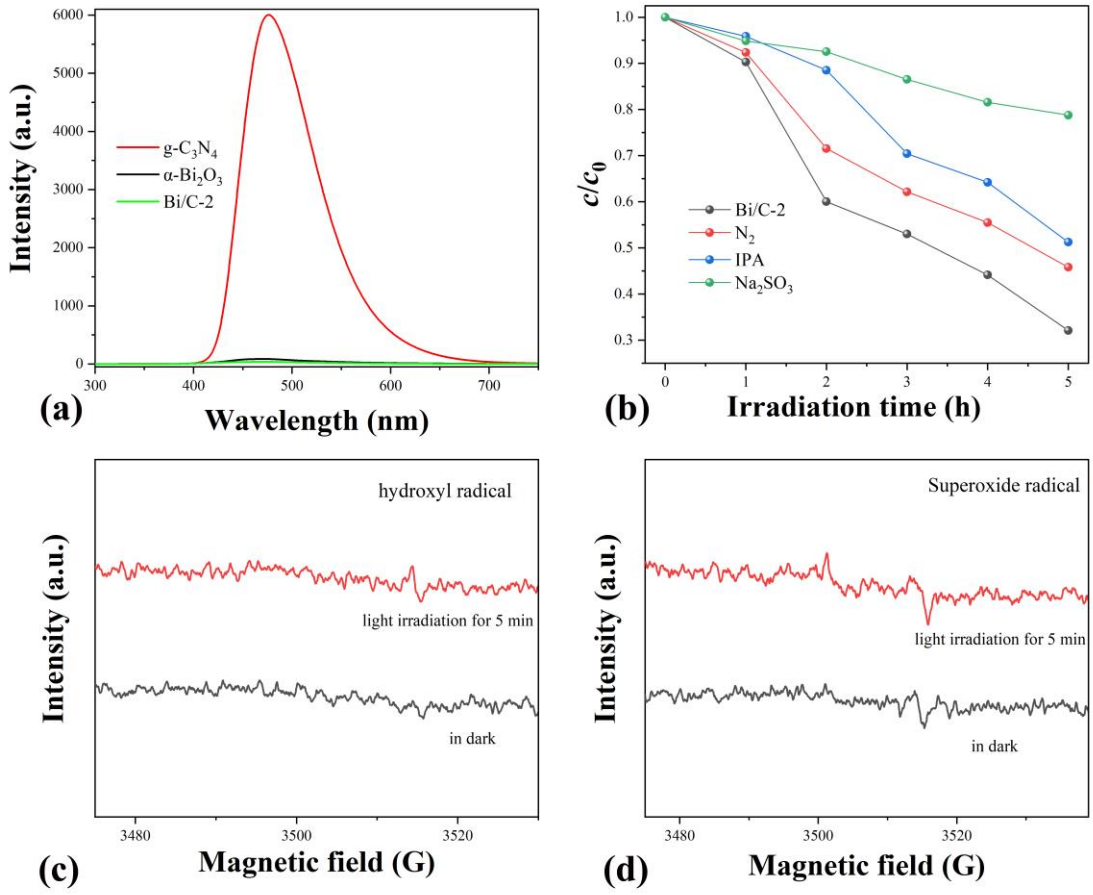

Fig. 9. PL spectra of g-C_3N_4, Bi_2O_3 and Bi/C-2 (a). Trapping experiment results of Bi/C-2 during the photodegradation progress of 2,4-DCP (b). ESR spectra of radical adducts trapped by DMPO; hydroxyl radical species detected for the Bi/C-2 dispersion in water (c) and superoxide radical species detected for the Bi/C-2 dispersions in methanol (d).

Afterword, the trapping experiment was also experimentalized to reveal the primary reactive species in the photodegradation. IPA and Na_2SO_3 are used as the scavengers

for hydroxyl radical and holes, respectively. N_2 purging is applied to dislodge the dissolved oxygen and stop forming superoxide radicals. As shown in Fig. 9b, when N_2 or IPA was introduced to the reaction system, the catalytic performance reduced to some extent. In comparison, when Na_2SO_3 was added, the photodegradation efficiency was significantly prohibited. The inhibiting effects follow an order of N_2 < IPA < Na_2SO_3. It can be concluded that the main active species in the photochemical reaction process of Bi/C-2 are oxidative holes, while hydroxyl radicals and superoxide radicals also contributed to the degradation of 2,4-DCP. In situ radical capture with ESR technique was employed to further confirm the active species of Bi/C-2. As shown in Fig .9c and d, no apparent signals of hydroxyl radicals or superoxide radicals were discovered either in dark or under light irradiation, suggesting the existence of minor amounts of free radicals or the rapid quenching between them. The dominant reactive species for the 2,4-DCP oxidation is mainly due to the direct oxidation between holes and pollutants.

In summary, the light absorption of Bi/C-2 is much stronger than that of Bi_2O_3 and g-C_3N_4. The enhanced photocurrent intensity and smaller EIS arc radius indicate the migration and separation of photogenerated charge carriers are greatly enhanced. Furthermore, the PL spectra can further illustrate the higher separating rate of electron and hole pairs. Hydroxyl radicals cannot be detected in ESR and the signal of superoxide radicals are quite weak, indicating hydroxyl radicals and superoxide radicals are not the dominant reactive oxygen species in the photooxidation. According to the results of trapping experiments, the photogenerated holes are the main active sites and accounted for 2,4-DCP degradation.

In this work, we report a facile synthesis of novel Bi/Bi_2O_3/C composite

photocatalyst for highly efficient 2,4-dichlorophenol degradation through the calcination of different ratios of bismuth nitrate pentahydrate and dicyandiamide. The photocatalytic activity of Bi/C-2 is demonstrated to be 1.60 times as Bi_2O_3 and 2.47 times as g-C_3N_4 for 2,4-dichlorophenol degradation, which is also highly stable with its photocatalytic activity did not decrease in four cycles. Previously, Au is used to modify Bi_2O_3 and improve its photocatalytic activity on the degradation of organic pollutants, however, Au is too expensive to be applied compared with the Bi/C-2 synthesized in this work.[47, 60-61] A lot of other Bi-based semiconductors, such as Bi_2S_3,[62] Bi_2WO_6,[63] $BiVO_4$,[64] $Bi_2O_2(OH)(NO_3)$,[65] BiOCl,[66] BiOBr,[67] BiOI and $Bi_{12}O_{17}Cl_{12}$[68] have also been used to photodegrade 2,4-dichlorophenol. While these Bi-based photocatalysts must be synthesized via solvothermal method, in which a large quantity of water and ethanol are needed to wash the product prepared. In addition, the waste liquids also contain uncertain ions that are probably to cause secondary pollution. In other work, even hypertoxic ethylene glycol is employed as the solution of solvothermal reaction, which is certainly not environmentally friendly. In contrast, the synthesis of Bi_2O_3 of this work is much more facile and environmentally friendly, with only calcination of bismuth nitrate being required without any further operation, which might facilitate the potential wide application of the novel photocatalyst for highly efficient 2,4-dichlorophenol degradation.

Based on the characterization and experimental results, the possible mechanism for the formation of the novel materials with enhanced photocatalytic activity (i.e., Bi/C-2) is proposed. When the mass ratio of bismuth nitrate pentahydrate and dicyandiamide is 4:1 or 1:1, the calcined product contains α-Bi_2O_3, metallic Bi and organic carbon. The thermal decomposition of dicyandiamide produced a large amount of ammonia that has

strong reducibility for reducing partial surface Bi^{3+} to Bi^0. If more dicyandiamide is used, more Bi metal can be obtained. The bismuth nitrate pentahydrate and its calcined product blocked the polymerization of dicyandiamide. Thus dicyandiamide cannot be transferred to g-C_3N_4 and but organic carbon. When the mass ratio of bismuth nitrate pentahydrate and dicyandiamide decreased to 2:3 or 1:4, the phase of α-Bi_2O_3 was transformed to β-Bi_2O_3. The incompletely polymerized dicyandiamide gradually coated on the surface of bismuth nitrate pentahydrate and limited the heat release of Bi_2O_3. As a result, the O layer became parallel to the x–y plane and high-temperature stable phase β-Bi_2O_3 is formed.[40] Although β-Bi_2O_3 has narrower bandgap and better photocatalytic activity than α-Bi_2O_3, the sample Bi/C-3 and Bi/C-4 contain too much inactive and incompletely polymerized dicyandiamide which severely limited the photocatalytic activity.

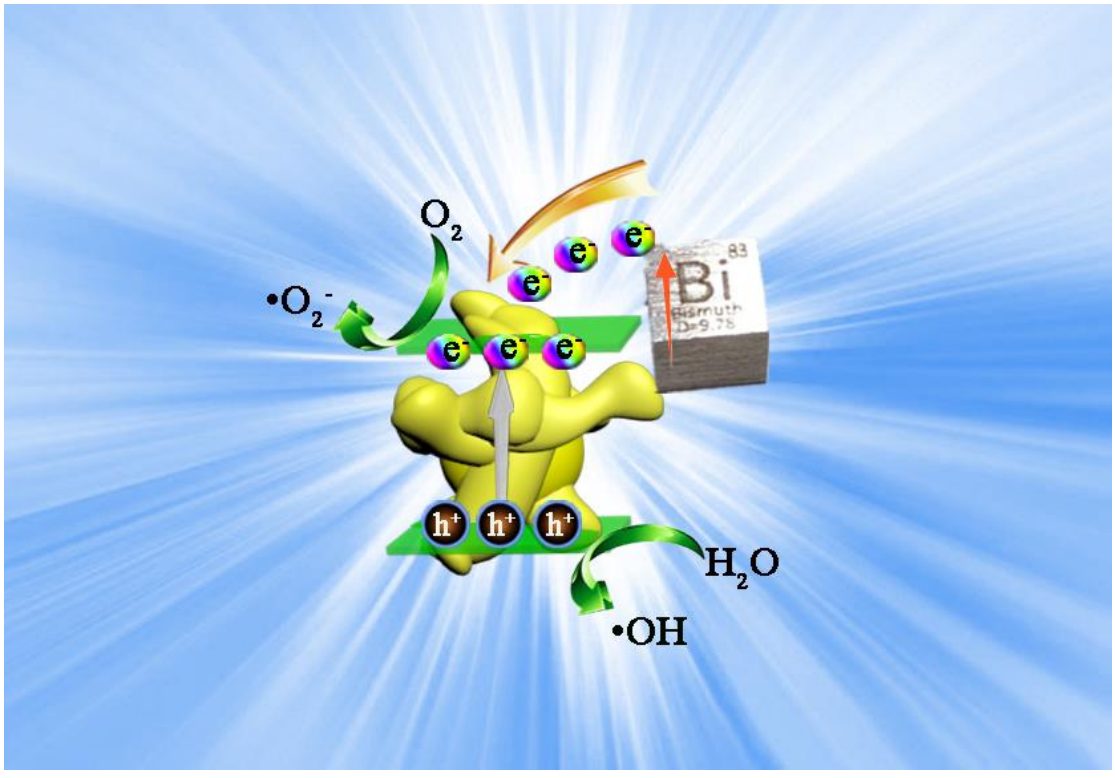

Fig. 10. Proposed mechanism for the enhanced photocatalytic activity of Bi/C-2

The photocatalytic mechanisms studies of this work further revealed that, under solar light irradiation, electrons in Bi_2O_3 are excited to the conduction band (CB) and holes on the valence band (VB) are produced. Electrons can react with oxygen and produce superoxide radicals, meanwhile holes can oxidize water to produce hydroxyl radicals or directly oxidize organic pollutants. Superoxide radicals, hydroxyl radicals and holes are all strong oxidizing species. However, the rapid recombination of electron and hole pairs limits the photocatalytic performance. Therefore, the three key mechanisms for the enhanced catalytic activity of the of the novel Bi/C-2 would include (Fig. 10) the following aspects: (1) When metallic Bi and carbon are induced to the composite, the composite materials possessed higher utilization ability of solar light, especially in the visible and infrared region; (2) Metallic Bi and carbon can improve the separation efficiency and transport of electron-hole pairs to generate reactive species for organic oxidation; and (3) The Fermi level of Bi is -0.17 eV and it is more negative than its CB. Under solar light irradiation, the electrons of Bi can be injected into the CB of Bi_2O_3. As a result, the population of photo-excited electrons and free radicals over the CB of Bi_2O_3 can be increased.

4. Conclusions

In summary, novel $Bi/Bi_2O_3/C$ composite was obtained via a facile synthesis of for highly efficient 2,4-dichlorophenol degradation by calcination of bismuth nitrate pentahydrate and dicyandiamide at different ratios. The photooxidation rate of Bi/C-2 is demonstrated to be 1.60-fold of Bi_2O_3 and 2.47-fold of g-C_3N_4 in 2,4-DCP degradation. The hybrid catalysts are also highly stable and the photocatalytic activity can be maintained in four successive cycles. The boosted photocatalytic performance

can be attributed to the enhanced light absorption, accelerated transfer and separation of photogenerated carriers and the SPR effect of metallic Bi and conductive carbon support. The main active species in the photochemical reaction process of Bi/C-2 are identified to be the oxidative holes, whereas hydroxyl radicals and superoxide radicals may also play auxiliary roles during the photodegradation.

Author information

Corresponding Author

***E-mail:** bingjieni@gmail.com

ORCID

Qiang Hao: 0000-0001-9981-7499

Yiwen Liu: 0000-0001-6677-7961

Author Contributions

The manuscript was written through contributions of all authors. All authors have given approval to the final version of the manuscript.

Notes

The authors declare no competing financial interest.

Acknowledgement

This work is supported by of an Australian Research Council (ARC) Future Fellowship (FT160100195). Yiwen Liu acknowledges the support from the UTS Chancellor's Postdoctoral Research Fellowship and CTWW Industry Partner & ECR Mentoring Scheme funding. The authors are grateful to the research collaboration.

References

1. Lee, L. S.; Rao, P. S. C.; Brusseau, M. L., Nonequilibrium Sorption and Transport of Neutral and Ionized Chlorophenols. *Environ. Sci. Technol.* **1991,** *25*, 722-729.

2. Contreras, S.; Rodriguez, M.; Al Momani, F.; Sans, C.; Esplugas, S., Contribution of the Ozonation Pre-treatment to the Biodegradation of Aqueous Solutions of 2,4-dichlorophenol. *Water Res.* **2003,** *37*, 3164-3171.

3. Munoz, M.; de Pedro, Z. M.; Casas, J. A.; Rodriguez, J. J., Chlorophenols Breakdown by a Sequential Hydrodechlorination-oxidation Treatment with a Magnetic Pd-Fe/gamma-Al_2O_3 Catalyst. *Water Res.* **2013,** *47*, 3070-3080.

4. Li, R. C.; Jin, X. Y.; Megharaj, M.; Naidu, R.; Chen, Z. L., Heterogeneous Fenton Oxidation of 2,4-dichlorophenol Using Iron-based Nanoparticles and Persulfate System. *Chem. Eng. J.* **2015,** *264*, 587-594.

5. Honda, M.; Kannan, K., Biomonitoring of Chlorophenols in Human Urine from Several Asian Countries, Greece and the United States. *Environ. Pollut.* **2018,** *232*, 487-493.

6. Kucuk, D.; Liman, R., Cytogenetic and Genotoxic Effects of 2-chlorophenol on Allium Cepa L. Root Meristem Cells. *Environ. Sci. Pollut. Res. Int.* **2018,** *25,* 36177-36123.

7. Tutem, E.; Apak, R.; Unal, C. F., Adsorptive Removal of Chlorophenols from Water by Bituminous Shale. *Water Res.* **1998,** *32*, 2315-2324.

8. Kalderis, D.; Kayan, B.; Akay, S.; Kulaksiz, E.; Gozmen, B., Adsorption of 2,4-dichlorophenol on Paper Sludge/Wheat Husk Biochar: Process Optimization and Comparison with Biochars Prepared from Wood Chips, Sewage Sludge and Hog Fuel/Demolition Waste. *J. Environ. Chem. Eng.* **2017,** *5*, 2222-2231.

9. Chen, C.; Geng, X.; Huang, W., Adsorption of 4-chlorophenol and Aniline by Nanosized Activated Carbons. *Chem. Eng. J.* **2017,** *327*, 941-952.

10. Sang, Y.; Zhao, Z.; Zhao, M.; Hao, P.; Leng, Y.; Liu, H., From UV to Near-Infrared, WS_2 Nanosheet: A Novel Photocatalyst for Full Solar Light Spectrum Photodegradation. *Adv. Mater.* **2015,** *27*, 363-369.

11. Zhou, Y. J.; Zhang, L. X.; Liu, J. J.; Fan, X. Q.; Wang, B. Z.; Wang, M.; Ren, W. C.; Wang, J.; Li, M. L.; Shi, J. L., Brand new P-doped g-C_3N_4: Enhanced Photocatalytic Activity for H-2 Evolution and Rhodamine B Degradation Under Visible Light. *J. Mater. Chem. A* **2015,** *3*, 3862-3867.

12. Weng, S. X.; Chen, B. B.; Xie, L. Y.; Zheng, Z. Y.; Liu, P., Facile in Situ Synthesis of a Bi/BiOCl Nanocomposite with High Photocatalytic Activity. *J. Mater. Chem. A* **2013,** *1*, 3068-3075.

13. Hao, Q.; Hao, S. M.; Niu, X. X.; Li, X.; Chen, D. M.; Ding, H., Enhanced Photochemical Oxidation Ability of Carbon Nitride by pi-pi Stacking Interactions with Graphene. *Chin. J. Catal.* **2017,** *38*, 278-286.

14. Ou, H. J.; Zhang, W. J.; Yang, X. F.; Cheng, Q. R.; Liao, G. Y.; Xia, H.; Wang, D. S., One-pot Synthesis of g-C_3N_4-doped Amine-rich Porous Organic Polymer for Chlorophenol Removal. *Environ.-Sci. Nano* **2018,** *5*, 169-182.

15. El-Maghrabi, H. H.; Barhoum, A.; Nada, A. A.; Moustafa, Y. M.; Seliman, S. M.; Youssef, A. M.; Bechelany, M., Synthesis of Mesoporous Core-shell CdS@TiO_2 (0D and 1D) Photocatalysts for Solar-driven Hydrogen Fuel Production. *J. Photochem. Photobiol. A-Chem.* **2018,** *351*, 261-270.

16. El-Maghrabi, H. H.; Al-Kahlawy, A. A.; Nada, A. A.; Zaki, T., Photocorrosion Resistant Ag_2CO_3@Fe_2O_3/TiO_2-NT Nanocomposite for Efficient Visible Light Photocatalytic Degradation Activities. *J. Hazard. Mater.* **2018,** *360*, 250-256.

17. Liu, Y.; Yao, W.; Liu, D.; Zong, R.; Zhang, M.; Ma, X.; Zhu, Y., Enhancement of Visible Light Mineralization Ability and Photocatalytic Activity of $BiPO_4$/BiOI. *Appl. Catal. B-Environ.* **2015,** *163*, 547-553.

18. Hao, Q.; Niu, X. X.; Nie, C. S.; Hao, S. M.; Zou, W.; Ge, J. M.; Chen, D. M.; Yao, W. Q., A Highly Efficient g-C_3N_4/SiO_2 Heterojunction: the Role of SiO_2 in the Enhancement of Visible Light Photocatalytic Activity. *Phys. Chem. Chem. Phys.* **2016,** *18*, 31410-31418.

19. Debono, O.; Hequet, V.; Le Coq, L.; Locoge, N.; Thevenet, F., VOC Ternary Mixture Effect on ppb Level Photocatalytic Oxidation: Removal Kinetic, Reaction Intermediates and Mineralization. *Appl. Catal. B-Environ.* **2017,** *218*, 359-369.

20. Jiang, L. B.; Yuan, X. Z.; Zeng, G. M.; Liang, J.; Wu, Z. B.; Wang, H.; Zhang, J.; Xiong, T.; Li, H., A Facile Band Alignment of Polymeric Carbon Nitride Isotype Heterojunctions for Enhanced Photocatalytic Tetracycline Degradation. *Environ.-Sci. Nano* **2018,** *5*, 2604-2617.

21. Deng, Y. C.; Tang, L.; Zeng, G. M.; Feng, C. Y.; Dong, H. R.; Wang, J. J.; Feng, H. P.; Liu, Y. N.; Zhou, Y. Y.; Pang, Y., Plasmonic Resonance Excited Dual Z-scheme $BiVO_4$/Ag/Cu_2O Nanocomposite: Synthesis and Mechanism for Enhanced Photocatalytic Performance in Recalcitrant Antibiotic Degradation. *Environ.-Sci. Nano* **2017,** *4*, 1494-1511.

22. Di, J.; Xia, J.; Ge, Y.; Li, H.; Ji, H.; Xu, H.; Zhang, Q.; Li, H.; Li, M., Novel Visible-light-driven CQDs/Bi_2WO_6 Hybrid Materials with Enhanced Photocatalytic Activity toward Organic Pollutants Degradation and Mechanism Insight. *Appl. Catal. B-Environ.* **2015,** *168*, 51-61.

23. Hao, Q.; Chen, T.; Wang, R.; Feng, J.; Chen, D.; Yao, W., A Separation-free Polyacrylamide/Bentonite/Graphitic Carbon Nitride Hydrogel with Excellent Performance in Water Treatment. *J. Clean. Prod.* **2018,** *197*, 1222-1230.

24. Saravanan, R.; Khan, M. M.; Gupta, V. K.; Mosquera, E.; Gracia, F.; Narayanan, V.; Stephen, A., ZnO/Ag/CdO Nanocomposite for Visible Light-induced Photocatalytic Degradation of Industrial Textile Effluents. *J. Colloid Interf. Sci.* **2015,** *452*, 126-133.

25. Xu, D.; Cheng, B.; Cao, S.; Yu, J., Enhanced Photocatalytic Activity and Stability of Z-scheme Ag_2CrO_4-GO Composite Photocatalysts for Organic Pollutant Degradation. *Appl. Catal. B-Environ.* **2015,** *164*, 380-388.

26. Jiang, N.; Lyu, L.; Yu, G. F.; Zhang, L. L.; Hu, C., A Dual-reaction-center Fenton-like Process on -C N-Cu Linkage Between Copper Oxides and Defect-containing g-C_3N_4 for Efficient Removal of Organic Pollutants. *J. Mater. Chem. A* **2018,** *6*, 17819-17828.

27. Schneider, J.; Matsuoka, M.; Takeuchi, M.; Zhang, J. L.; Horiuchi, Y.; Anpo, M.; Bahnemann, D. W., Understanding TiO_2 Photocatalysis: Mechanisms and Materials. *Chem. Rev.* **2014,** *114*, 9919-9986.

28. Lee, K. M.; Lai, C. W.; Ngai, K. S.; Juan, J. C., Recent Developments of Zinc Oxide Based Photocatalyst in Water Treatment Technology: A Review. *Water Res.* **2016,** *88*, 428-448.

29. Zhu, Y.; Ling, Q.; Liu, Y.; Wang, H.; Zhu, Y., Photocatalytic Performance of $BiPO_4$ Nanorods Adjusted via Defects. *Appl. Catal. B-Environ.* **2016,** *187*, 204-211.

30. Schultz, D. M.; Yoon, T. P., Solar Synthesis: Prospects in Visible Light Photocatalysis. *Science* **2014,** *343*, 1239176.

31. Li, X.; Liu, P.; Mao, Y.; Xing, M.; Zhang, J., Preparation of Homogeneous Nitrogen-doped Mesoporous TiO_2 Spheres with Enhanced Visible-light Photocatalysis. *Appl. Catal. B-Environ.* **2015,** *164*, 352-359.

32. Kang, Y.; Yang, Y.; Yin, L.-C.; Kang, X.; Wang, L.; Liu, G.; Cheng, H.-M., Selective Breaking of Hydrogen Bonds of Layered Carbon Nitride for Visible Light Photocatalysis. *Adv. Mater.* **2016,** *28*, 6471-

6477.
33. Lv, Y. H.; Liu, Y. F.; Zhu, Y. Y.; Zhu, Y. F., Surface Oxygen Vacancy Induced Photocatalytic Performance Enhancement of a $BiPO_4$ Nanorod. *J. Mater. Chem. A* **2014,** *2*, 1174-1182.
34. Wan, Z.; Zhang, G. K., Synthesis and Facet-dependent Enhanced Photocatalytic Activity of Bi_2SiO_5/AgI Nanoplate Photocatalysts. *J. Mater. Chem. A* **2015,** *3*, 16737-16745.
35. Wu, Y.; Yuan, B.; Li, M.; Zhang, W.-H.; Liu, Y.; Li, C., Well-defined BiOCl Colloidal Ultrathin Nanosheets: Synthesis, Characterization, and Application in Photocatalytic Aerobic Oxidation of Secondary Amines. *Chem. Sci.* **2015,** *6*, 1873-1878.
36. Yu, Y.; Cao, C. Y.; Liu, H.; Li, P.; Wei, F. F.; Jiang, Y.; Song, W. G., A Bi/BiOCl Heterojunction Photocatalyst with Enhanced Electron-hole Separation and Excellent Visible Light Photodegrading Activity. *J. Mater. Chem. A* **2014,** *2*, 1677-1681.
37. Hao, Q.; Wang, R.; Lu, H.; Xie, C. a.; Ao, W.; Chen, D.; Ma, C.; Yao, W.; Zhu, Y., One-pot Synthesis of C/Bi/Bi_2O_3 Composite with Enhanced Photocatalytic Activity. *Appl. Catal. B-Environ.* **2017,** *219*, 63-72.
38. Bian, Z.; Zhu, J.; Wang, S.; Cao, Y.; Qian, X.; Li, H., Self-assembly of Active Bi_2O_3/TiO_2 Visible Photocatalyst with Ordered Mesoporous Structure and Highly Crystallized Anatase. *J. Phys. Chem. C* **2008,** *112*, 6258-6262.
39. Hameed, A.; Montini, T.; Gombac, V.; Fornasiero, P., Surface Phases and Photocatalytic Activity Correlation of Bi(2)O(3)/Bi(2)O(4-x) Nanocomposite. *J. Am. Chem. Soc.* **2008,** *130*, 9658-9659.
40. Lu, H.; Hao, Q.; Chen, T.; Zhang, L.; Chen, D.; Ma, C.; Yao, W.; Zhu, Y., A high-performance Bi_2O_3/Bi_2SiO_5 p-n Heterojunction Photocatalyst Induced by Phase Transition of Bi_2O_3. *Appl. Catal. B-Environ.* **2018,** *237*, 59-67.
41. Reddy, J. K.; Srinivas, B.; Kumari, V. D.; Subrahmanyam, M., Sm^{3+}-Doped Bi_2O_3 Photocatalyst Prepared by Hydrothermal Synthesis. *Chemcatchem* **2009,** *1*, 492-496.
42. Wu, X.; Qin, W.; Li, L.; Guo, Y.; Xie, Z., Photocatalytic Property of Nanostructured Fe^{3+}-doped Bi_2O_3 Films. *Catal. Commun.* **2009,** *10*, 600-604.
43. Chai, S. Y.; Kim, Y. J.; Jung, M. H.; Chakraborty, A. K.; Jung, D.; Lee, W. I., Heterojunctioned BiOCl/Bi_2O_3, a new Visible Light Photocatalyst. *J. Catal.* **2009,** *262*, 144-149.
44. Bessekhouad, Y.; Robert, D.; Weber, J. V., Photocatalytic Activity of CU_2O/TiO_2, Bi_2O_3/TiO_2 and $ZnMn_2O_4$/TiO_2 Heterojunctions. *Catal. Today* **2005,** *101*, 315-321.
45. Lin, X.; Xing, J.; Wang, W.; Shan, Z.; Xu, F.; Huang, F., Photocatalytic Activities of Heterojunction Semiconductors Bi_2O_3/$BaTiO_3$: A Strategy for the Design of Efficient Combined Photocatalysts. *J. Phys. Chem. C* **2007,** *111*, 18288-18293.
46. Hsieh, S. H.; Lee, G. J.; Chen, C. Y.; Chen, J. H.; Ma, S. H.; Horng, T. L.; Chen, K. H.; Wu, J. J., Synthesis of Pt Doped Bi_2O_3/RuO_2 Photocatalysts for Hydrogen Production from Water Splitting Using Visible Light. *J. Nanosci. Nanotechno.* **2012,** *12*, 5930-5936.
47. Anandan, S.; Lee, G.-J.; Chen, P.-K.; Fan, C.; Wu, J. J., Removal of Orange II Dye in Water by Visible Light Assisted Photocatalytic Ozonation Using Bi_2O_3 and Au/Bi_2O_3 Nanorods. *Ind. Eng. Chem. Res.* **2010,** *49*, 9729-9737.
48. Li, Y.; Zhang, Z.; Zhang, Y.; Sun, X.; Zhang, J.; Wang, C.; Peng, Z.; Si, H., Preparation of Ag Doped Bi_2O_3 Nanosheets with Highly Enhanced Visible Light Photocatalytic Performances. *Ceram. Int.* **2014,** *40*, 13275-13280.
49. Dong, F.; Xiong, T.; Sun, Y. J.; Zhao, Z. W.; Zhou, Y.; Feng, X.; Wu, Z. B., A Semimetal Bismuth Element as a Direct Plasmonic Photocatalyst. *Chem. Commun.* **2014,** *50*, 10386-10389.

50. He, W. J.; Sun, Y. J.; Jiang, G. M.; Li, Y. H.; Zhang, X. M.; Zhang, Y. X.; Zhou, Y.; Dong, F., Defective Bi_4MoO_9/Bi Metal Core/Shell Heterostructure: Enhanced Visible Light Photocatalysis and Reaction Mechanism. *Appl. Catal. B-Environ.* **2018,** *239*, 619-627.

51. He, W. J.; Sun, Y. J.; Jiang, G. M.; Huang, H. W.; Zhang, X. M.; Dong, F., Activation of Amorphous Bi_2WO_6 with Synchronous Bi Metal and Bi_2O_3 Coupling: Photocatalysis Mechanism and Reaction Pathway. *Appl. Catal. B-Environ.* **2018,** *232*, 340-347.

52. Yu, S.; Huang, H.; Dong, F.; Li, M.; Tian, N.; Zhang, T.; Zhane, Y., Synchronously Achieving Plasmonic Bi Metal Deposition and I- Doping by Utilizing $BiOIO_3$ as the Self-Sacrificing Template for High-Performance Multifunctional Applications. *ACS Appl. Mater. Inter.* **2015,** *7*, 27925-27933.

53. Wang, J.; Tang, L.; Zeng, G.; Liu, Y.; Zhou, Y.; Deng, Y.; Wang, J.; Peng, B., Plasmonic Bi Metal Deposition and g-C_3N_4 Coating on Bi_2WO_6 Microspheres for Efficient Visible-Light Photocatalysis. *ACS Sustain. Chem. Eng.* **2017,** *5*, 1062-1072.

54. Huang, Y. K.; Kang, S. F.; Yang, Y.; Qin, H. F.; Ni, Z. J.; Yang, S. J.; Li, X., Facile Synthesis of Bi/Bi_2WO_6 Nanocomposite with Enhanced Photocatalytic Activity under Visible Light. *Appl. Catal. B-Environ.* **2016,** *196*, 89-99.

55. Dong, F.; Zhao, Z. W.; Sun, Y. J.; Zhang, Y. X.; Yan, S.; Wu, Z. B., An Advanced Semimetal-Organic Bi Spheres-g-C_3N_4 Nanohybrid with SPR-Enhanced Visible-Light Photocatalytic Performance for NO Purification. *Environ. Sci. Technol.* **2015,** *49*, 12432-12440.

56. Lee, W. H.; Lee, J. G.; Reucroft, P. J., XPS Study of Carbon Fiber Surfaces Treated by Thermal Oxidation in a Gas Mixture of O-2/(O-2+N-2). *Appl. Surf. Sci.* **2001,** *171*, 136-142.

57. Yang, H. F.; Li, F. H.; Shan, C. S.; Han, D. X.; Zhang, Q. X.; Niu, L.; Ivaska, A., Covalent Functionalization of Chemically Converted Graphene Sheets via Silane and its Reinforcement. *J. Mater. Chem.* **2009,** *19*, 4632-4638.

58. Kwan, Y. C. G.; Ng, G. M.; Huan, C. H. A., Identification of Functional Groups and Determination of Carboxyl Formation Temperature in Graphene Oxide Using the XPS O 1s Spectrum. *Thin Solid Films* **2015,** *590*, 40-48.

59. Liu, X. W.; Cao, H. Q.; Yin, J. F., Generation and Photocatalytic Activities of Bi@Bi_2O_3 Microspheres. *Nano Res.* **2011,** *4*, 470-482.

60. Jiang, H. Y.; Cheng, K.; Lin, J., Crystalline Metallic Au Nanoparticle-Loaded alpha-Bi_2O_3 Microrods for Improved Photocatalysis. *Phys. Chem. Chem. Phys.* **2012,** *14*, 12114-12121.

61. Pugazhenthiran, N.; Sathishkumar, P.; Murugesan, S.; Anandan, S., Effective Degradation of Acid Orange 10 by Catalytic Ozonation in the Presence of Au-Bi_2O_3 Nanoparticles. *Chem. Engi. J.* **2011,** *168*, 1227-1233.

62. Zhou, J.; Tian, G. H.; Chen, Y. J.; Shi, Y. H.; Tian, C. G.; Pan, K.; Fu, H. G., Growth Rate Controlled Synthesis of Hierarchical Bi_2S_3/In_2S_3 Core/Shell Microspheres with Enhanced Photocatalytic Activity. *Sci Rep* **2014,** *4*, 4321.

63. Lv, Y.; Yao, W.; Zong, R.; Zhu, Y., Fabrication of Wide-Range-Visible Photocatalyst Bi_2WO_6-x Nanoplates via Surface Oxygen Vacancies. *Sci Rep* **2016,** *6,* 19347.

64. Zhou, B.; Zhao, X.; Liu, H. J.; Qu, J. H.; Huang, C. P., Synthesis of Visible-Light Sensitive M-$BiVO_4$ (M = Ag, Co, and Ni) for the Photocatalytic Degradation of Organic Pollutants. *Sep. Purif. Technol.* **2011,** *77* , 275-282.

65. Huang, H.; He, Y.; Li, X.; Li, M.; Zeng, C.; Dong, F.; Du, X.; Zhang, T.; Zhang, Y., $Bi_2O_2(OH)(NO_3)$ as a Desirable Bi_2O_2 (2+) Layered Photocatalyst: Strong Intrinsic Polarity, Rational Band Structure and {001} Active Facets Co-beneficial for Robust Photooxidation Capability. *J. Mater. Chem. A* **2015,** *3*,

24547-24556.
66. Cheng, H.; Huang, B.; Qin, X.; Zhang, X.; Dai, Y., A Controlled Anion Exchange Strategy to Synthesize Bi_2S_3 Nanocrystals/BiOCl Hybrid Architectures with Efficient Visible Light Photoactivity. *Chem. Commun.* **2012,** *48*, 97-99.
67. Chen, S.; Yan, R.; Zhang, X.; Hu, K.; Li, Z.; Humayun, M.; Qu, Y.; Jing, L., Photogenerated Electron Modulation to Dominantly Induce Efficient 2,4-dichlorophenol Degradation on BiOBr Nanoplates with Different Phosphate Modification. *Appl. Catal. B-Environ.* **2017,** *209*, 320-328.
68. Huang, H.; Xiao, K.; He, Y.; Zhang, T.; Dong, F.; Du, X.; Zhang, Y., In Situ Assembly of BiOI@$Bi_{12}O_{17}Cl_2$ p-n Junction: Charge Induced Unique Front-lateral Surfaces Coupling Heterostructure with High Exposure of BiOI {001} Active Facets for Robust and Nonselective Photocatalysis. *Appl. Catal. B-Environ.* **2016,** *199*, 75-86.

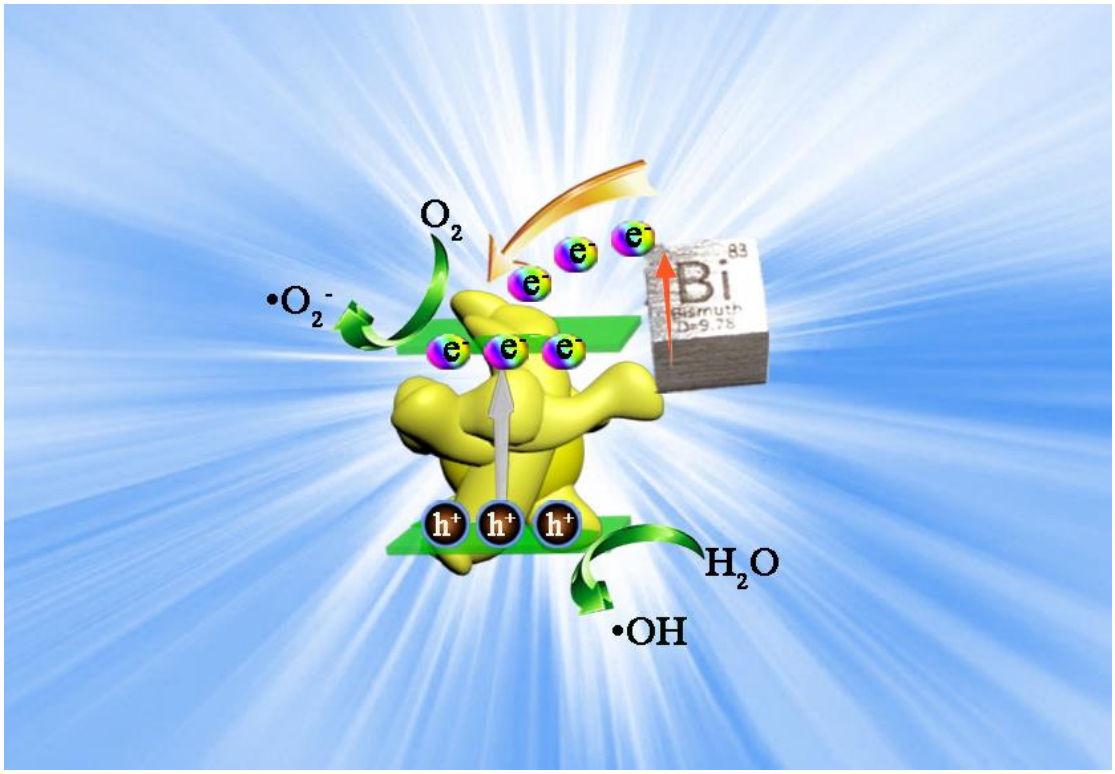

TOC

Supporting Information

Bi_2O_3@Carbon Nanocomposites for Solar-Driven Photocatalytic Degradation of Chlorophenols

Qiang Hao†, Yiwen Liu†, Tong Chen‡, Qingfeng Guo§, Wei Wei†, and Bing-Jie Ni*†

†Centre for Technology in Water and Wastewater (CTWW), School of Civil and Environmental Engineering, University of Technology Sydney (UTS), Sydney, NSW 2007, Australia

‡ School of Materials Science and Technology and § School of Gemmology, China University of Geosciences Beijing. Beijing, 100083, China

***Corresponding author:**

Tel.: +61 295147401; E-mail: bingjieni@gmail.com

1. Characterizations

XRD patterns of the samples were obtained from a D/max-2400 X-ray diffractometer at 25 °C with intense Cu *K*α radiation and the operation voltage was 40 kV. Fourier transform infrared spectroscopy (FTIR) was tested by a Bruker V70 Fourier transform infrared spectrometer from the wavenumber of 4000-600 cm^{-1} which did not need the use of potassium bromide (KBr) as blank background. X-ray photoelectron spectroscopy (XPS) measurements were from a PHI Quantera XPS with Al *K*α radiation resource and it was operated at 40 W. JEOL2100F thermal field high resolution transmission electron microscope (HRTEM) was employed to test the morphology and structure of Bi/C-2. A Hitachi U-3900 scan UV–vis spectrophotometer was applied to test the UV-vis diffuse reflectance spectroscopy (DRS) of prepared samples, using high purity barium sulfate ($BaSO_4$) as the standard reference. Photoluminescence (PL) spectra were obtained from a Hitachi F-4600 fluorescence spectrometer excited at 325 nm. Photocurrent and electrochemical impedance spectroscopy (EIS) were tested with a CHI 760E electrochemical workstation in 0.1 M Na_2SO_4 solution. The counter electrode was a Pt wire, and the reference electrode was a saturated calomel electrode (SCE). The working electrodes were prepared as follow: 5 mg of samples and 1 mL ethanol were mixed in 5 mL cuvettes; after that the cuvettes were sonicated for 4 h to disperse the samples in the solvent homogeneously; then the suspension was evenly coated on indium-tin oxide (ITO) glasses (5 × 2 cm) and dried in air for 12 h. When testing photocurrent, the light was provided by a 300 W xenon lamp (PLS-SXE-300) and its intensity was 40 mW/cm^2, besides no voltage was used. EIS was tested in the frequency from 1 to 1×10^5 Hz the initial voltage was 0 V and the amplitude was 0.005 V. A Bruker ESR 300E was employed to test the electron spin resonance (ESR) spectra of Bi/C-2 and *5*,*5*-dimethyl-*1*-pyrroline *N*-oxide (DMPO) was

used as the radical scavenger.

2. Photocatalytic activity tests

The photocatalytic activity of prepared samples was evaluated for degradation of 2,4-DCP in aqueous solution. The photocatalytic reaction test was carried out with a PhchemIII photochemical reactions instrument and the light resource was a 500 W xenon lamp with an average light intensity of 35 mW/cm^2. The light intensity was tested by a FZ-A radiometer (Beijing Perfectlight Technology Co,Ltd). Firstly, 50 mg of samples were weight and put in a 50 mL quartz cuvette. Then 50 mL 2,4-DCP solution (10 ppm) was added to the cuvette. The mixture was kept in dark and strongly stirred for 2 h to reach the adsorption-desorption equilibrium. After that, 3 ml of suspension was sampled and the light was turned on. With the light on and magnetically stirring, the photocatalytic reaction lasted for 5 h and 3 ml of suspension was sampled per hour. High-performance liquid chromatography (HPLC) (Shimadzu LC-20AT) was used to measure the concentration of 2,4-DCP. Before measurement, all the suspension samples were filtered by 0.45 μm micropore filter. The mobile phase was methanol and water (volume ratio: 75/25), the elution time was 5.5 min, the flow rate was 1 mL/min, the determining wavelength was 284 nm and the chromatographic column was a Venusil XBP-C18 (3.9 × 200, Agela Technologies Inc.) column.